Journal of Systems Engineering and Electronics
Vol. 31, No. 4, August 2020, pp.657 – 665

Joint synchronization estimation based on genetic algorithm for OFDM/OQAM systems

LIU Yongjin*, CHEN Xihong, and ZHAO Yu

Air and Missile Defense College, Air Force Engineering University, Xi'an 710051, China

Abstract: This paper investigates the problem of synchronization for offset quadrature amplitude modulation based orthogonal frequency division multiplexing (OFDM/OQAM) systems based on the genetic algorithm. In order to increase the spectrum efficiency, an improved preamble structure without guard symbols is derived at first. On this basis, instead of deriving the log likelihood function of power spectral density, joint estimation of the symbol timing offset and carrier frequency offset based on the preamble proposed is formulated into a bivariate optimization problem. After that, an improved genetic algorithm is used to find its global optimum solution. Conclusions can be drawn from simulation results that the proposed method has advantages in the joint estimation of synchronization.

Keywords: offset quadrature amplitude modulation based orthogonal frequency division multiplexing (OFDM/OQAM), synchronization, joint estimation, genetic algorithm.

DOI: 10.23919/JSEE.2020.000041

1. Introduction

Due to the advantages in resistance to inter-symbol interference and inter-carrier interference, offset quadrature amplitude modulation based orthogonal frequency division multiplexing (OFDM/OQAM) has become the candidate of 5th-generation (5G) modulation [1]. However, because there are no cyclic prefix inserted in OFDM/OQAM systems, symbol time offset (STO) will lead to malposition during fast Fourier transformation (FFT) and cause block interference, carrier frequency offset (CFO) will destroy the orthogonality between carriers and cause difficulty in correct demodulation of the systems [2]. Furthermore, channel estimation and even the performance of the whole system is related to STO and CFO. Therefore, joint STO and CFO estimation for the OFDM/OQAM systems should be valued.

Manuscript received August 07, 2019.

*Corresponding author.

This work was supported by the National Natural Science Foundation of China (61671468).

In recent years, the problem of synchronization for OFDM/OQAM systems has attracted more and more attention. All these methods can be divided into two classes: data-aided methods and blind methods. Regarding the blind methods, Fusco proved the conjugate-symmetry property of received signals in the frequency selective channel, which was then used to estimate CFO in [3]. The weakness of this method is the low convergence speed. Similarly, the approximate conjugate-symmetry property was also utilized by Mattera and Tanda to estimate the synchronization of the systems blindly in [4]. Moreover, signal characteristics were taken full advantage of in [5] to blindly estimate CFO of the doubly-selective fading channels. However, methods aforementioned can be further improved with respect to convergence speed and computational complexity.

Regarding the data-aided methods, Singh and Vasudevan adopted cross correlation and preamble respectively to estimate the coarse synchronization and the fine CFO in [6]. In [7], the fine CFO estimation in the Rayleigh fading channels was also achieved based on the interference approximate method. Synchronization was estimated based on the zero autocorrelation code in [8], whose preamble included two symbol intervals.

The synchronization results of the aforementioned data-aided methods are closely related to the preamble structures. Therefore, how to improve the preamble structure is very important in the data-aided synchronization algorithms. In [9], guard symbols were placed at two sides, instead of the same side of reference preamble symbols to modify the preamble structure. However, the spectrum of the system would be reduced due to the guard symbols. For the purpose of overcoming this defect, pilot symbols were coded to carry information that need to be transmitted in [10] to save the system spectrum. However, there are two symbol intervals in the preamble which can be further improved. In [11], a preamble with less spectrum consumption was proposed. In order to increase the transmission ef-

ficiency of the system, an efficient preamble structure was designed in this paper according to the thought proposed in [11].

Furthermore, data-aided synchronization algorithms mentioned above need at least two steps to estimate STO and CFO. There is so much preprocessing before the final estimation. It causes complex calculation. The genetic algorithm (GA) is able to solve this difficulty and has the ability to deal with both continuous and discontinuous functions [12].

There have been many researches on GA [13 – 19] recently. The main features of GA are the fast convergence speed and the optimal answer [20,21]. As a computerized search, GA was used by Kakandikar and Nandedkar in [22] to predict and optimize the thinning in automotive sealing cover. In [23], Podlena and Hendtlass proposed an improved GA based on the history network to speed up the convergence. The weakness of this method lies in the existence of random operators. Parents are chosen randomly in the selection operator. Chromosomes change randomly in the mutation operator. The directed random search (DRS) which is used to narrow the search space also depends on the random change of an individual. In addition, updating the exemplar stored in the history network is by merging the old exemplar with the current input randomly. GA will converge slowly with all these random operators. In [24], Seyyed and Samane adopted the pruning operator to avoid the random assignment of the value. In this paper, the GA with the pruning operator is adopted to speed up the convergence and search for the optimal answer.

In this paper, joint estimation of STO and CFO based on the preamble is formulated into an optimization problem, whose objective is to minimize the mean square error (MSE) caused by CFO and STO. After that, the pruning operator is used to improve the GA and find the global solution of the optimization problem.

Contributions of this paper are two-fold:

(i) Preamble structure design

A novel structure of the preamble is designed to save the system spectrum. Zero symbols are generally inserted between preambles and data symbols. In this study, preambles without zero symbols are considered to increase the transmission efficiency.

(ii) Synchronization problem formulation

Generally, power spectral density (PSD) of the system is derived before the log likelihood function is adopted to estimate STO and CFO. Instead, in this paper, joint STO and CFO estimation is straightly formulated as bivariate optimization to reduce calculations.

This paper is organized as follows. In Section 2, the OFDM/OQAM system model is described and the preamble structure is designed. In Section 3, joint STO and CFO estimation is formulated as bivariate optimization and the GA with the pruning operator is used to solve this optimization problem. In Section 4, simulation results are presented. Finally, conclusions are drawn in Section 5.

2. System model

Fig. 1 shows the model of the OFDM/QAM system [25]. $C2R_0$ represents converting complex signals into real signals. $R2C_0$ represents converting real signals into complex signals. $F_0(z)$ is the modulation filter function. $Q_0(z)$ is the demodulation filter function. $H(z)$ represents the channel impulse response. $\eta[k]$ represents the noise. The baseband equivalent of the discrete-time OFDM/OQAM transmitting signal can be written as

$$s[k]=\sum_{n=-\infty}^{+\infty}\sum_{m=0}^{M-1}\underbrace{\theta_{m,n}d_{m,n}}_{y_{m,n}}f_m\left[k-\frac{nM}{2}\right]\mathrm{e}^{\frac{-\mathrm{j}2\pi km}{M}} \quad (1)$$

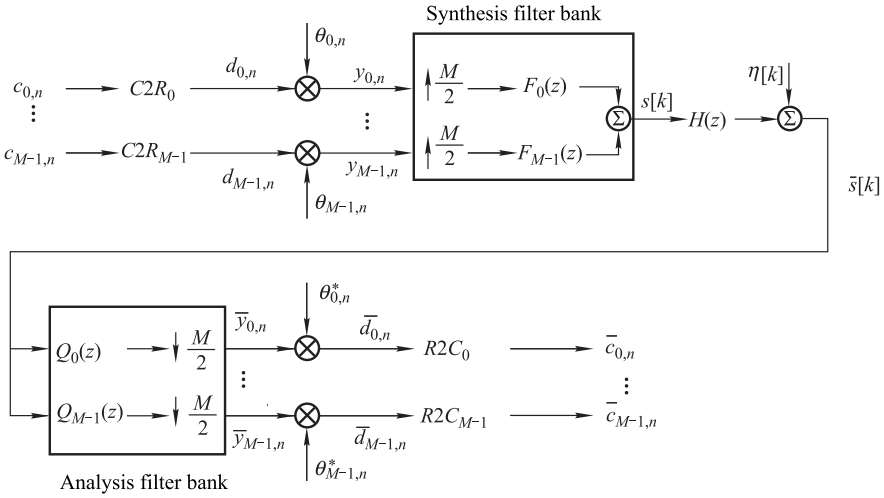

Fig. 1 OFDM/OQAM system model

where M, n, $m \in \{0, 1, \ldots, M-1\}$, $c_{m,n}$ and $d_{m,n}$ represent the number of subcarriers, the time index, the frequency index, the input symbols and the real valued OQAM symbols, respectively. $y_{m,n} = \theta_{m,n} d_{m,n}$, $\theta_{m,n} = \mathrm{j}^{m+n}$ and filter $f_m[k]$ satisfies

$$f_m[k] = G[k] \mathrm{e}^{\mathrm{j}\frac{2\pi m}{M}\left(k - \frac{L_p - 1}{2}\right)} \tag{2}$$

where $G[k]$ represents the prototype filter whose length is L_p.

The perfect reconstruction condition of the signal $\chi_{m,n}[k]$ satisfies

$$\Re\left\{\sum_{k=-\infty}^{+\infty} \chi_{m,n}[k], \chi^*_{m',n'}[k]\right\} = \delta_{m,m'}\delta_{n,n'} \tag{3}$$

where $\Re\{\cdot\}$ is the operation of taking the real part, $(\cdot)^*$ represents the complex conjugate, $\delta_{m,m'}$ denotes the Dirac's delta function, and

$$\chi_{m,n}[k] = \theta_{m,n} f_m\left[k - \frac{nM}{2}\right] \mathrm{e}^{\frac{-\mathrm{j}2\pi km}{M}}. \tag{4}$$

The preamble structure proposed in [26] is shown in Fig. 2. It can be seen from Fig. 2 that there are w columns of zero symbols.

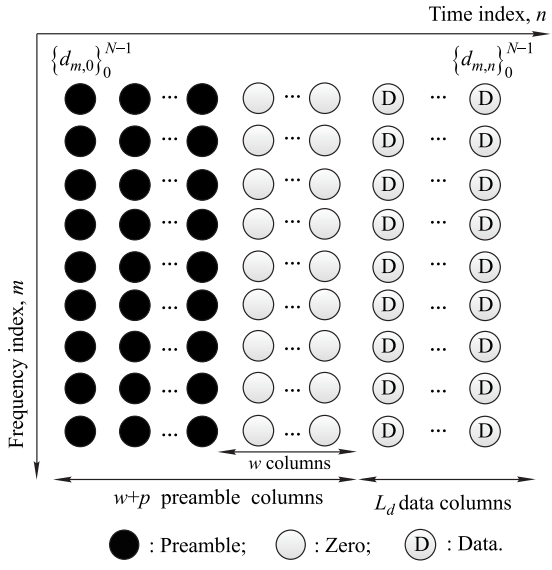

Fig. 2 Preamble structure proposed in [6]

According to [27], the continuous-time signal $s(k)$ can be described as

$$s(k) = \sigma_s \sum_{n=-\infty}^{N-1} [s^R_{k-nM,n} + \mathrm{j}s^I_{k-nM,n}], \tag{5}$$

$$s^R_{m,n} \triangleq \frac{1}{\sqrt{2}} \sum_{l=0}^{M-1} y^R_{l,n} \mathrm{e}^{\mathrm{j}\frac{2\pi}{M}lm} g(m), \tag{6}$$

$$s^I_{m,n} \triangleq \frac{1}{\sqrt{2}} \sum_{l=0}^{M-1} y^I_{l,n} \mathrm{e}^{\mathrm{j}\frac{2\pi}{M}lm} g\left(m + \frac{M}{2}\right), \tag{7}$$

where $\sigma_s^2 = \mathrm{E}[|s(k)|^2]$, $y^R_{l,n}$ is the real part of the complex data symbols and $y^I_{l,n}$ is the imaginary part, and $g(m)$ is the continuous form of the prototype filter which is the one proposed by Bellanger in [28].

The ambiguity function of $g(m)$ is defined as

$$A_g(\tau, \nu) = \int g\left(t + \frac{\tau}{2}\right) g^*\left(t - \frac{\tau}{2}\right) \mathrm{e}^{\mathrm{j}2\pi\nu t} \mathrm{d}t \tag{8}$$

where ν denotes the subcarrier spacing and τ denotes the symbol duration.

The relationship of the discrete-time signal $s[k]$ and the continuous-time signal $s(k)$ is $s^R(kT_s) \triangleq s^R[k]$, where T_s is the sampling period.

Define $C_{p,q} = \mathrm{j}^{p+q+pq+2pn_0} A_g(-q\tau, p\nu)$, and $\Omega^*_{\Delta m_0, \Delta n_0} = \Omega_{\Delta m_0, \Delta n_0} - (0,0)$, where $\Omega_{\Delta m_0, \Delta n_0}$ denotes the neighborhood of position (m_0, n_0). $C_{p,q}$ gradually approaches to zero along with the increasing of $|p|$ and $|q|$. For example, for the prototype filter of the isotropic orthogonal transform algorithm (IOTA), when $(p,q) \notin \Omega_{1,1}$, we have [29]

$$\frac{\sum\limits_{(p,q)\notin\Omega_{1,1}} |C_{p,q}|^2}{\sum\limits_{(p,q)\in\Omega^*_{1,1}} |C_{p,q}|^2} \approx 0.02. \tag{9}$$

Conclusion can be drawn from (9) that one column of guard symbols is adequate to prevent the pilot symbol from the interference. If there is only one column of guard symbols in the preamble, its channel estimation (CE) performance will be worse than that of the interference approximation method (IAM) [30]. As shown in Fig. 3, two columns of zero symbols are inserted in IAM.

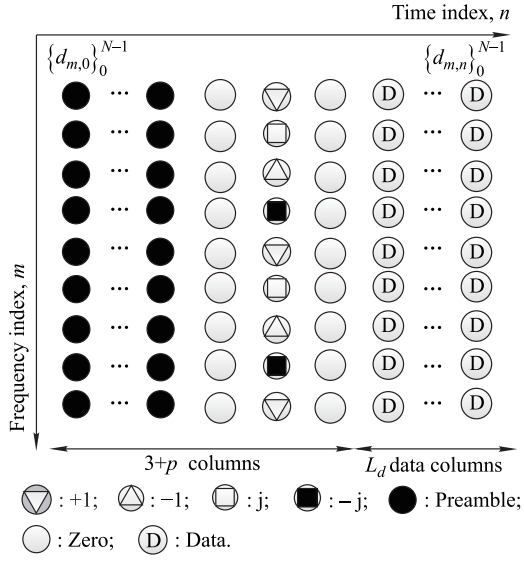

Fig. 3 Structure of IAM

According to [11], a higher power of the pseudo pilot means a better performance of CE. The power of pseudo pilot y' for the IAM is

$$E_1\{|y'_{m_0,n_0}|^2\} =$$

$$y^2_{m_0,n_0} + |C_{-1,0}y_{m_0-1,n_0} + C_{1,0}y_{m_0+1,n_0}|^2. \quad (10)$$

Obviously, there are two columns of zero symbols, which leads to the low spectrum efficiency. In order to increase the pseudo pilot power and spectrum efficiency, a preamble without zero symbols is proposed in this paper. The proposed structure of the preamble is shown in Fig. 4. Three-tap interferences are taken into account in this paper due to sufficient accuracy.

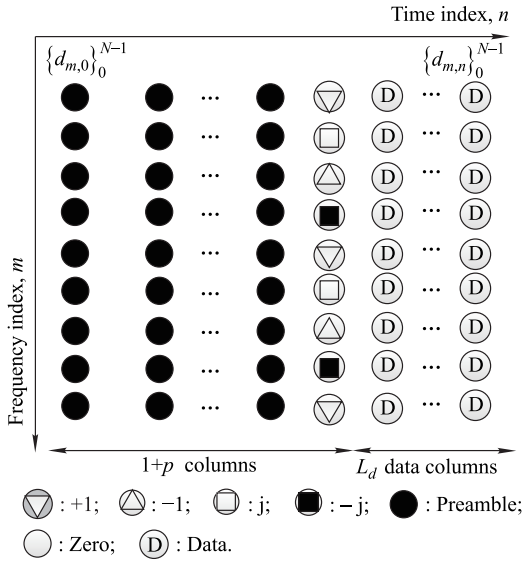

Fig. 4 The proposed structure for OQAM system

The power of pseudo pilot y' for the proposed structure in Fig. 4 can be written as

$$E_2\{|y'_{m_0,n_0}|^2\} = y^2_{m_0,n_0} +$$

$$\left| \sum_{(p,q)\in\Omega^*_{3,3}} C_{p,q}y_{m_0+p,n_0+q} \right|^2 > E_1\{|y'_{m_0,n_0}|^2\}. \quad (11)$$

Conclusion can be drawn from (11) that the structure proposed in Fig. 4 can increase the power of the pseudo pilot. It means that the structure proposed in Fig. 4 has the ability to decrease the interference caused by the adjacent unknown data symbol.

3. Joint estimation of CFO and STO

3.1 Problem formulation

Considering the additive white Gaussian noise (AWGN) channel with a zero-mean $\eta[k]$ which is statistically independent of $s[k]$, when the transmitted signals pass through this channel, the received signal $r[k]$ [6] is written as

$$r[k] = s[k-\tau_0]\mathrm{e}^{\mathrm{j}\frac{2\pi\mu_0 k}{M}} + \eta[k] \quad (12)$$

where τ_0 is STO corresponding to one half of a symbol duration and μ_0 is normalized CFO corresponding to the sub-channel frequency spacing, $\mu_0 \in [-\Delta, \Delta]$. Assume that Δ is known to the receiver.

According to the previous researches, the second-order effects of STO and CFO are negligible, which therefore can be neglected in the OFDM/OQAM system model [31].

The demodulation signal at preamble position (m_0, n_0) is

$$\widehat{y}_{m_0,n_0} = \sum_{k=-\infty}^{+\infty} r[k]\chi^*_{m_0,n_0}[k] =$$

$$\sum_{k=-\infty}^{+\infty} \mathrm{e}^{\mathrm{j}\frac{2\pi\mu_0 k}{M}} \sum_{n=0}^{p+L_d} \sum_{m=0}^{M-1} y_{m,n}G[k-\tau_0-nM]\cdot$$

$$G[k-n_0M]\cdot \mathrm{e}^{-\mathrm{j}\frac{2\pi\tau_0 m}{M}}\mathrm{e}^{\frac{2\pi}{M}(m-m_0)\left(k-\frac{L_p-1}{2}\right)} +$$

$$\underbrace{\sum_{k=-\infty}^{+\infty} \eta[k]\chi^*_{m_0,n_0}[k]}_{\eta_{m_0,n_0}}. \quad (13)$$

where we define $\eta_{m_0,n_0} = \sum_{k=-\infty}^{+\infty} \eta[k]\chi^*_{m_0,n_0}[k]$.

For the preamble symbols $\{d_{m,0}\}_0^{N-1}$, when $0 \leqslant m_0 \leqslant M-1$, (13) can be rewritten as

$$\widehat{y}_{m_0,0} = \mathrm{e}^{\mathrm{j}\frac{2\pi\mu_0 k}{M}}[y_{m_0,0}\mathrm{e}^{-\mathrm{j}\frac{2m_0\pi}{M}\tau_0} \sum_{k=\tau_0}^{L_p-1} p[k]p[k-\tau_0] +$$

$$\sum_{\substack{m=0\\ m\neq m_0}}^{M-1} y_{m,0}\mathrm{e}^{-\mathrm{j}\frac{2m\pi}{M}\tau_0} \sum_{k=\tau_0}^{L_p-1} p[k]p[k-\tau_0]\cdot$$

$$\mathrm{e}^{\mathrm{j}\frac{2\pi}{M}(m-m_0)\left(k-\frac{L_p-1}{2}\right)}] + \eta_{m_0,0}. \quad (14)$$

Equation (14) implies that the demodulation of the preamble signal is composed of two parts: the first term presents the interference caused by the surrounding symbols, the second term is the transmitted signal $y_{m_0,0}$ plus attenuation. It means that CFO and STO will introduce interference into the demodulation process. In this section, the MSE is derived to describe the influence of the interference caused by CFO and STO.

Define

$$z_i = y_{i,0}\mathrm{e}^{-\mathrm{j}\frac{2\pi i}{M}\tau_0} \sum_{k=\tau_0}^{L_p-1} p[k]p[k-\tau_0] +$$

$$\sum_{\substack{m=0\\m\neq i}}^{M-1} y_{i,0}\mathrm{e}^{-\mathrm{j}\frac{2\pi m}{M}\tau_0}\sum_{k=\tau_0}^{L_p-1} p[k]p[k-\tau_0]\mathrm{e}^{\mathrm{j}\frac{2\pi}{M}(m-i)\left(k-\frac{L_p-1}{2}\right)}. \tag{15}$$

Rewrite (14) in vector notation as

$$\boldsymbol{Y} = \mathrm{e}^{\mathrm{j}\frac{2\pi k}{M}\mu_0}\boldsymbol{Z} + \boldsymbol{\zeta} \tag{16}$$

where $\boldsymbol{\zeta}$ is the noise vector, and

$$\begin{cases} \boldsymbol{Y} = [\widehat{y}_{0,0} \quad \widehat{y}_{1,0} \quad \cdots \quad \widehat{y}_{M-1,0}]^{\mathrm{T}} \\ \boldsymbol{Z} = [z_0 \quad z_1 \quad \cdots \quad z_{M-1}]^{\mathrm{T}} \\ \boldsymbol{\zeta} = [\eta_{0,0} \quad \eta_{1,0} \quad \cdots \quad \eta_{M-1,0}] \end{cases}. \tag{17}$$

Considering zero-mean AWGN $\eta[k]$ with variance δ^2, the covariance matrix of $\boldsymbol{\zeta}$ is

$$\boldsymbol{C}_{\boldsymbol{\zeta}} = \delta^2 \begin{pmatrix} 1 & \Psi_{0,0}^{1,0} & \cdots & \Psi_{0,0}^{M-1,0} \\ \Psi_{1,0}^{0,0} & 1 & \cdots & \Psi_{1,0}^{M-1,0} \\ \vdots & \vdots & \ddots & \vdots \\ \Psi_{M-1,0}^{0,0} & \Psi_{M-1,0}^{1,0} & \cdots & 1 \end{pmatrix} \tag{18}$$

where $\Psi_{q,0}^{p,0} = \mathrm{cov}[\eta_{p,0}, \eta_{q,0}^*]$.

According to [32], the MSE can be written as

$$\mathrm{MSE} = Tr\Big\{\Big[\big(\boldsymbol{Y} - \mathrm{e}^{\mathrm{j}\frac{2\pi k}{M}\mu_0}\boldsymbol{Z}\big)^{\mathrm{H}}\boldsymbol{C}_{\boldsymbol{\zeta}}^{-1}\big(\boldsymbol{Y} - \mathrm{e}^{\mathrm{j}\frac{2\pi k}{M}\mu_0}\boldsymbol{Z}\big) + \boldsymbol{C}_{\boldsymbol{\zeta}}^{-1}\Big]^{-1}\Big\}. \tag{19}$$

Therefore, the joint CFO and STO are formulated into bivariate optimization as follows:

$$\min_{\mu_0,\tau_0} Tr\Big\{\Big[\big(\boldsymbol{Y} - \mathrm{e}^{\mathrm{j}\frac{2\pi k}{M}\mu_0}\boldsymbol{Z}\big)^{\mathrm{H}}\boldsymbol{C}_{\boldsymbol{\zeta}}^{-1}\big(\boldsymbol{Y} - \mathrm{e}^{\mathrm{j}\frac{2\pi k}{M}\mu_0}\boldsymbol{Z}\big) + \boldsymbol{C}_{\boldsymbol{\zeta}}^{-1}\Big]^{-1}\Big\}.$$

3.2 Problem solution

GA is a powerful tool to deal with complicated issues and optimization problems. There are many advantages of GA over other techniques, such as the ability to obtain the global optimal answer rather than local optima. The global optimal answers are all contained in the search space which may be expanded by gorges in GA. Furthermore, the space that does not contain answers may cause redundant search, which will slow down the convergence speed of GA.

In [23], Podlena and Hendtlass utilized the history network to store the record of spaces that already have been searched. In this way, the redundant repetition can be avoided in the same generation. For the next generation, the history network will be inquired before iteration about whether the space has been searched. This function is called Baldwin effect. It can be seen that Baldwin effect is able to avoid the redundant search in invalid space. However, Podlena and Hendtlass have not attached importance to the random operators in GA, which probably causes early termination of iteration and even the wrong solution. In [24], Seyyed and Samane applied the pruning operator to avoid the random assignment of the value. There is much in their method that can be used. In order to speed up the convergence, the pruning operator can be adopted to improve the method proposed by Podlena and Hendtlass. In this paper, the pruning operator and the history network are combined with each other to improve the GA.

The time order of the pruned initialization is shown in

$$\text{Initialization} = O(N_p \cdot N_g \cdot N_c) \tag{20}$$

where N_c represents the number of chromosomes of each generation, N_g represents the number of genomes in each chromosome, and N_p is determined by the pruning function. It is shown in

$$N_p = \begin{cases} \eta, & \eta \leqslant N_g \cdot N_c \\ N_g \cdot N_c, & \eta > N_g \cdot N_c \end{cases} \tag{21}$$

where η is the reduced ratio of the search space.

The time order of the pruned search loop is shown in (22), where N_s represents the solution space.

$$\text{Search loop} = O\left(\frac{N_s}{\eta} \cdot N_c^2 \cdot N_p\right) \tag{22}$$

4. Simulation results

4.1 Performance of the proposed preamble

In this section, the CE performance based on the proposed preamble structure is simulated. Truncation of an IOTA filter with length $4T_0$ [33] is chosen as the prototype filter in this simulation. The fundamental parameters are listed in Table 1 where ITU is the International Telecommunications Union.

Table 1 Fundamental parameters of CE

Parameter	Value
Subcarrier spacing/kHz	$\nu_0 = 10.94$
Filter length	$L_g = 4M + 1$
Channel coding	Convolution coding
Channel mode	ITU Vehicular B [34]
Channel path delay/μs	[0, 1.6, 3.5, 5.0]
Frame length	20 OQAM symbols

Fig. 5 illustrates the CE performances of two methods for different kinds of constellation mapping. For convergence, the proposed structure in this paper is named as

A and the IAM is named as B. For 16-QAM modulation, a higher signal to noise ratio (SNR) means a better CE performance and B shows worse CE performance than A when SNR<15 dB. The reason is that there are imaginary preamble symbols in the proposed structure to increase the pseudo pilot power. Additionally, because there exists a performance platform, curves of B become flatten when SNR>15 dB. For 4-QAM modulation, the similar phenomenon occurs when SNR>20 dB.

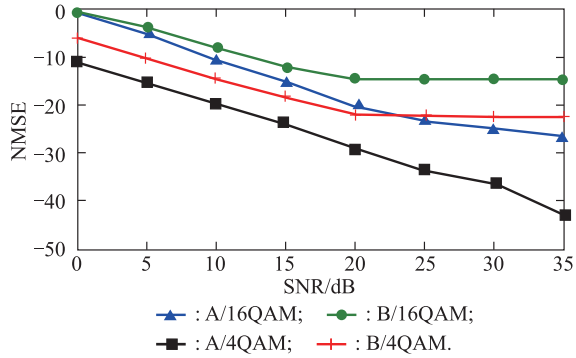

Fig. 5 Normalized MSE (NMSE) performance of the proposed structure A and the IAM structure B for 4-QAM and 16-QAM in CE

In Fig. 6, the CE performance of two methods are compared with each other when the number of subcarriers are respectively 256 and 512. For structure A, the curve with 512 subcarriers is lower than that with 256 subcarriers. Curves of structure B show the same results. It implies that a larger number of subcarriers means a better CE performance. Furthermore, it can be seen from Fig. 6 that when $\mathrm{BER} = 10^{-3}$, structure A with 256 subcarriers and 512 subcarriers are respectively better than that of structure B about 0.4 dB and 1 dB, which proves that structure A has better CE performance than structure B.

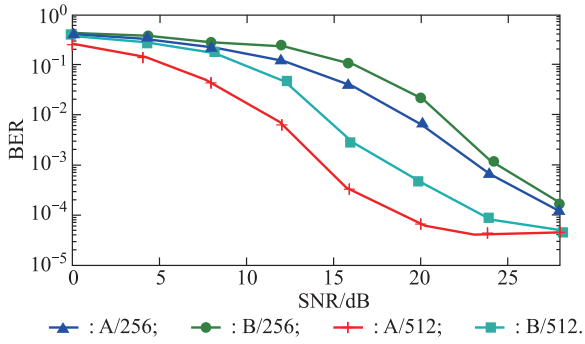

Fig. 6 Bit error ratio (BER) performance of the proposed structure A and the IAM structure B for different numbers of subcarriers in CE

4.2 Performance of the synchronization method

The fundamental parameters are listed in Table 2.

Table 2 Fundamental parameters of synchronization estimation

Parameter	Value
Number of independent Monte Carlo trails	10^4
Bandwidth/MHz	$B = \dfrac{1}{T_s} = 11.2$
Subcarrier	$M \in \{1\,024, 2\,048, 4\,096\}$
Overlap parameter	$k = 4$
The overall interval length	$10M$
Channel mode	ITU Vehicular A and ITU Vehicular B [34]

Fig. 7, Fig. 8 and Fig. 9 respectively show the performance of the STO estimation on different channels for different numbers of subcarriers. The purpose of analyzing the coarse estimation is to be compared with the proposed STO estimation method. In Fig. 7, it is obvious that the performance of the proposed method is superior to the coarse procedure on the ITU-A and ITU-B channels. The proposed method achieves a better performance on channel ITU-A than the coarse estimation on the AWGN channel.

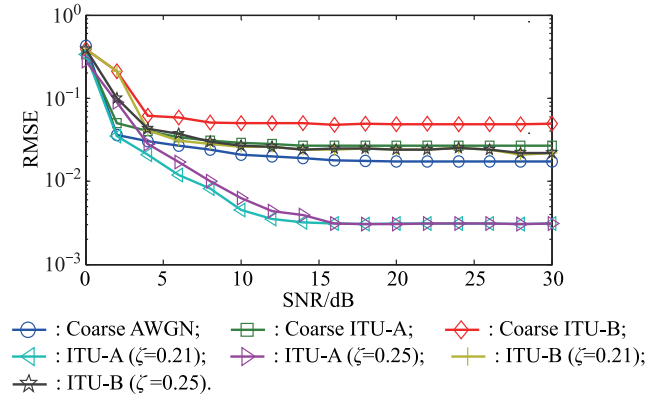

Fig. 7 Performance of the STO estimation in different channels for M=1 024

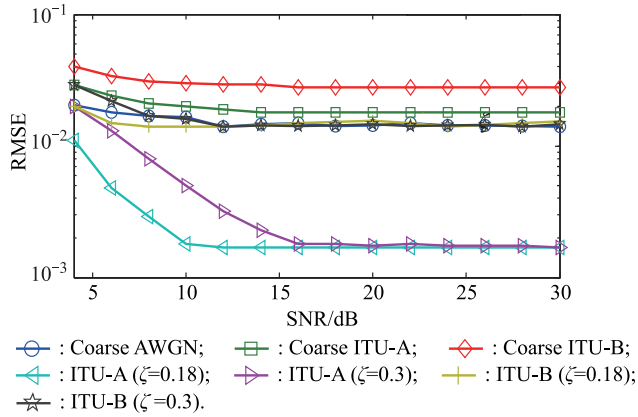

Fig. 8 Performance of the STO estimation on different channels for M=2 048

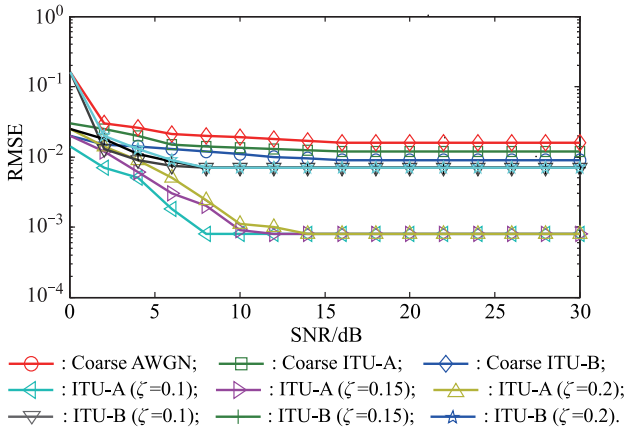

Fig. 9 Performance of the STO estimation on different channels for M=4 096

For the same channel, a larger value of the threshold means a worse performance. Moreover, the convergence speed of the proposed method on channel ITU-A is slower than that on ITU-B and AWGN. The reason is that the ITU-A channel model is with mobility, time variation of the channel will be enhanced, and Doppler spread and Doppler shift will become obvious with the increased mobility. The lines in Fig. 8 have the same tendency as that in Fig. 7. Comparing Fig. 9 with Fig. 7 and Fig. 8, the effect of the number of subcarriers on the performance of the proposed estimation method can be analyzed. A larger number of subcarriers means a better estimation performance.

The CFO estimation performances of three methods in different simulation environments are compared with each in Fig. 10, Fig. 11 and Fig. 12. For convenience, methods proposed in [9], [19] and this paper are respectively named as method A, method B and method C. The computer simulations in Fig. 11 show that the performance of CFO estimation in the context of the AWGN channel is the best while that in the context of channel ITU-B is the worst, no matter which method is used. For one certain method, the performance gap between different channels is more obvious when SNR>10 dB due to the multipath effects. In the context of the AWGN channel, method C is the best one to estimate CFO while the rest two methods show the similar performance, especially when SNR>14 dB. Things are different when it comes to the rest two channels, method A becomes the best one and there exist intersections between different lines. The performance gap between different lines is more obvious when SNR>20 dB. Furthermore, a larger SNR always means a better CFO estimation performance for whichever simulation environment. In conclusion, the method proposed in this paper is effective in different simulation environments and has outperformance in the CFO estimation domain. Similar conclusion can be drawn from Fig. 10 and Fig. 12.

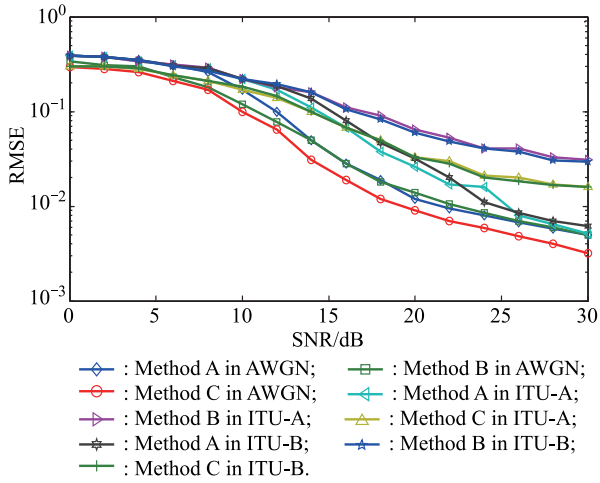

Fig. 10 Performance of the three CFO estimators on different channels for M=1 024

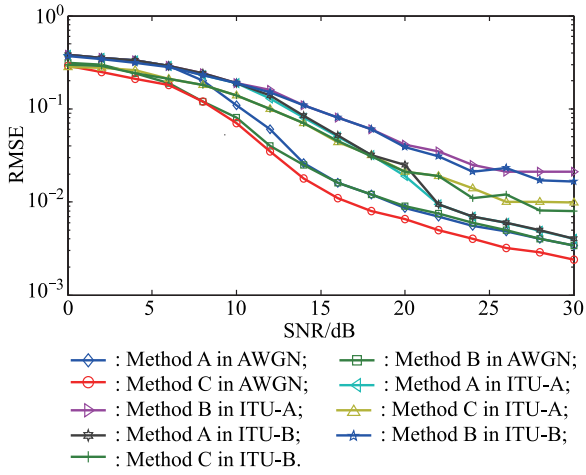

Fig. 11 Performance of the three CFO estimators on different channels for M=2 048

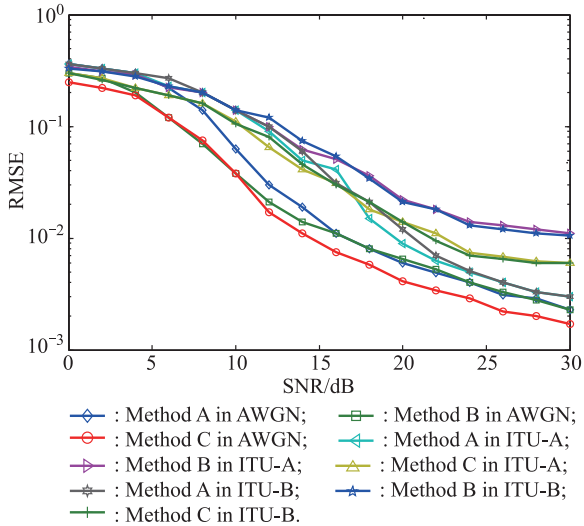

Fig. 12 Performance of the three CFO estimators on different channels for M=4 096

The sensitivity of the OFDM/OQAM system to the STO and CFO directly results in the poor BER performance. In order to better verify the advantages of the proposed synchronization estimation method, BER performance of the proposed synchronization estimation method is compared with the improved data-aided joint CFO and time offset estimation method in [35]. Fig. 13 shows that the proposed method has a better BER performance than that in [35]. When SNR=10 dB, the method proposed in this paper is better than the method in [35] by about 1.3 dB. The gap becomes larger with the increase of SNR. It can be seen from Fig. 4 that pilot symbols +1, −1, j and −j are alternately set in the preamble structure proposed in this paper. In this structure, the interference around pilot symbols will be cancelled by each other. Therefore, the proposed structure can reduce the inter-symbol interference and increase the pseudo pilot power. Furthermore, the accuracy of the synchronization estimation will be increased and the BER performance will be better than other methods.

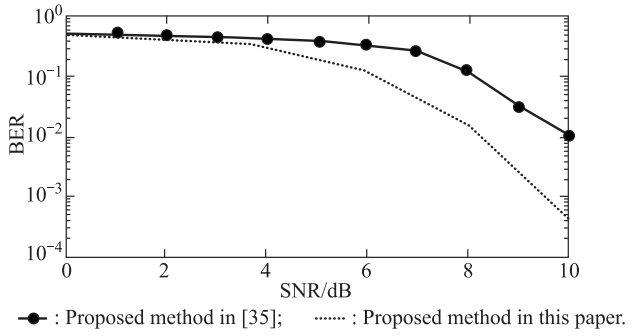

Fig. 13 BER performance of the methods proposed in this paper and [35]

5. Conclusions

This paper investigates the joint estimation of STO and CFO based on an improved GA for OFDM/OQAM systems. Specially, a new preamble structure without zero symbols is proposed at first to increase the spectral efficiency. On this basis, the MSE caused by CFO and STO is derived. The joint CFO and STO estimation is formulated into a bivariate optimization problem, and minimizing the MSE is treated as the objective. Furthermore, the pruning operator is used to improved GA and find the global solution of this optimization problem. Simulations results show that STO and CFO can be jointly estimated by the proposed method with acceptable performance. Because the preamble proposed in this paper carries no information and GA belongs to the evolutionary algorithm, how to code the pilot to improve the data transmission speed and utilize other evolutionary algorithms in joint synchronization estimation are the directions for future improvement.

References

[1] LI J, TIAN Y, QIU Y, et al. Principles, technologies and challenges of OQAM-OFDM for 5G applications. Telecommunications Science, 2016, 32(6): 1571 – 1575.
[2] LIN H, GHAHA M, SILHAN P. Impact of time and carrier frequency offsets on the FBMC/OQAM modulation scheme. Signal Processing, 2014, 102(2): 151 – 162.
[3] FUSCO T, TANDA M. Blind frequency-offset estimation for OFDM/OQAM systems. IEEE Trans. on Signal Processing, 2007, 55(2): 1828 – 1838.
[4] MATTERA D, TANDA M. Blind symbol timing and CFO estimation for OFDM/OQAM systems. IEEE Trans. on Wireless Communications, 2013, 12(1):268 – 277.
[5] ZHAO Y, CHEN X H. Blind CFO estimation for OFDM/OQAM systems over doubly-selective fading channels. Journal of Communications, 2015, 10(5): 301 – 307.
[6] SINGH P, VASUDEVAN K. Preamble-based synchronization for OFDM/OQAM systems in AWGN channel. Proc. of the 4th International Conference on Signal Processing and Integrated Networks, 2017: 60 – 65.
[7] SINGH P, VASUDEVAN K. Frequency synchronization and channel estimation for OFDM/OQAM signals transmitted through Rayleigh fading channels. Proc. of the 23rd National Conference on Communications, 2017. DOI: 10.1109/NCC.2017.8077048.
[8] QIAN X W, DENG Y S, DENG H G, et al. Synchronization algorithm for OFDM/OQAM systems based on zero autocorrelation code. IET Communication, 2018, 12(3): 283 – 289.
[9] HU S, WU G, YANG G, et al. Effectiveness of preamble based channel estimation for OFDM/OQAM system. Proc. of the International Conference on Networks Security, Wireless Communications and Trusted Computing, 2009, 1: 34 – 37.
[10] CUI W J, QU D M, JIANG T. Code auxiliary pilots for channel estimation in FBMC-OQAM systems. IEEE Trans. on Vehicular Technology, 2016, 65(5): 2936 – 2946.
[11] CHENG G B, XIAO Y, HU S, et al. Interference cancellation aided channel estimation for OFDM/OQAM system. Science China (Information Sciences), 2013, 56(12): 1 – 8.
[12] NAZARAHARI M, KHANMIRZA E, DOOSTIE S. Multi-objective multi-robot path planning in continuous environment using an enhanced genetic algorithm. Expert Systems with Applications, 2019, 115: 106 – 120.
[13] RAJABI M, SHAFIEI F. QSAR models for predicting aquatic toxicity of esters using genetic algorithm-multiple linear regression methods and molecular descriptors. Combinatorial Chemistry & High Throughput Screening, 2019, 22(5): 317 – 325.
[14] FANG Y Q, XIAO X, GE J W. Cloud computing task scheduling algorithm based on improved genetic algorithm. Proc. of the 3rd Information Technology, Networking, Electronic and Automation Control Conference, 2019. DOI: 10.1109/ITNEC.2019.8728996.
[15] QU X Z, LIU G P, DUAN S Y, et al. Multi-objective robust optimization method for the modified epoxy resin sheet molding compounds of the impeller. Journal of Computational Design and Engineering, 2016, 3(3): 179 – 190.
[16] MARANDI R A, HU M, CHOWDHURY S. A system of system approach for smart complex energy system operation decision. Proc. of the ASME International Design Engineering Technical Conferences and Computers and Information in Engineering Conference, 2015. DOI: 10.1115/DETC2015-47415.
[17] JAFARI-MARANDI R, HU M Q, OMITAOMU O A. A distributed decision framework for building clusters with different

heterogeneity settings. Applied Energy, 2016, 165: 393 – 404.
[18] ZHAO J, CHEN J Q, XU L. RBF-GA: an adaptive radial basis function metamodeling with genetic algorithm for structural reliability analysis. Reliability Engineering and System Safety, 2019, 189: 42 – 57.
[19] SONG W, HUANG C M. Mining high utility item sets using bio-inspired algorithms: a diverse optimal value framework. IEEE Access, 2018, 6(1): 19568 – 19582.
[20] KURI-MORALES A, BOBADILLA E A. The best genetic algorithm I: a comparative study of structurally different genetic algorithms. Proc. of the 12th Mexican International Conference on Artificial Intelligence, 2013: 1 – 15.
[21] DOLDGERG D E. Genetic algorithms in search, optimization & machine learning. India: Pearson Education Pvt. Ltd, 2003.
[22] KAKANDIKAR G M, NANDEDKAR V M. Prediction and optimization of thinning in automotive sealing cover using genetic algorithm. Journal of Computational Design and Engineering, 2016, 3(1): 63 – 70.
[23] PODLENA J R, HENDTLASS T. An accelerated genetic algorithm. Applied Intelligence, 1998, 8(2): 103 – 111.
[24] SEYYED M H, SAMANE S M. Pruned genetic algorithm. Lecture Notes in Computer Science, 2010, 6320(1): 193 – 200.
[25] VIHOLAINEN A, IHALAINEN T, STITZ H, et al. Prototype filter design for filter bank based multicarrier transmission. Proc. of the 17th European Signal Processing Conference, 2009, 17: 1359 – 1363.
[26] LELE C, LEGOUABLE R, SIOHAN P. Channel estimation with scattered pilots in OFDM/OQAM. Proc. of the IEEE 9th Workshop on Signal Processing Advances in Wireless Communications, 2008: 286 – 290.
[27] SIOHAN P, SICLET C, LACAILLE N. Analysis and design of OFDM/OQAM systems based on filterbank theory. IEEE Trans. on Signal Processing, 2002, 50(5): 1170 – 1183.
[28] BELLANGER M. Specification and design of a prototype filter for filter bank based multicarrier transmissions. Proc. of the IEEE International Conference on Acoustics, Speech, and Signal Processing, 2001: 2417 – 2420.
[29] LELE C, SIOHAN P, LEGOUABLE R, et al. Preamble-based channel estimation techniques for OFDM/OQAM over the powerline. Proc. of the IEEE International Symposium on Power Line Communications and Its Applications, 2007: 59 – 64.
[30] VIHOLAINEN A, IHALAINEN T, STITZ T, et al. Prototype filter design for filter bank based multicarrier transmission. Proc. of the 17th European Signal Processing Conference, 2009: 1359 – 1363.
[31] FLOCH B L, ALARD M, BERROU C. Coded orthogonal frequency division multiplex. Proceedings of the IEEE, 1995, 83(6): 982 – 996.
[32] KAY S M. Fundamentals of stochastic signal processing: estimation theory. Englewood Cliffs: Prentice-Hall, 1993.
[33] BAGHAKI A, CHAMPAGNE B. Joint carrier frequency offset, sampling time offset and channel estimation for OFDM-OQAM systems. Proc. of the IEEE Wireless Communications and Networking Conference, 2018. DOI: 10.1109/WCNC.2018.8377020.
[34] International Telecommunication Union. Guidelines for evaluation of radio transmission technologies for IMT-2000: Recommendation ITU-R M. 1225. 1997. https://www.itu.int/rec/R-REC-M.1225-0-199702-1/en.
[35] XUE L S, QIU S F, WU P, et al. Improved data-aided joint carrier frequency offset and time offset estimation method for OFDM/OQAM system. Proc. of the IEEE 18th International Conference on Communication Technology, 2018. DOI: 10.1109/ICCT.2018.8600048.

Biographies

LIU Yongjin was born in 1990. He received his B.S. and M.S. degrees in armament science and technology from Air force Engineering University in 2014 and 2017 respectively. He is currently pursuing his Ph.D. degree in Air force Engineering University, Xi'an, China. His research interests include wireless communications, synchronization and dilter design for OFDM/OQAM systems and troposcatter com munication.
E-mail: liuyongjinDW@163.com

CHEN Xihong was born in 1961. He received his M.S. degree in communication engineering from Xidian University, Xi'an, in 1992 and Ph.D. degree from the Missile College of Air Force Engineering University (AFEU) in 2010. He is a professor with the Air and Missile Defense College, AFEU, Xi'an. His research interests include information theory, information security and signal processing.
E-mail: xhchen0315217@163.com

ZHAO Yu was born in 1989. He received his M.S. degree and Ph.D. degree in 2011 and 2015, respectively, from Air Force Engineering University (AFEU), Xi'an. He is currently doing postdoctoral research on electrical science and technology at the Air and Missile Defense College, AFEU. His research interests include information theory, multicarrier modulation techniques and deep learning in physical layer of wireless communications.
E-mail: 13636810730@163.com